Vision-Inspection-Synchronized Dual Optical Coherence Tomography for High-Resolution Real-Time Multidimensional Defect Tracking in Optical Thin Film Industry

DEOKMIN JEON[1], UNSANG JUNG[2], KIBEOM PARK[3], PILUN KIM[4], SANGYEOB HAN[1], HYOSANG JEONG[1], RUCHIRE ERANGA WIJESINGHE[5,8], NARESH KUMAR RAVICHANDRAN[6], JAEYUL LEE[1], YOUNGMIN HAN[7], MANSIK JEON[1], (Member, IEEE), AND JEEHYUN KIM[1], (Member, IEEE)

[1]School of Electronic and Electrical Engineering, College of IT Engineering, Kyungpook National University, Daegu 41566, South Korea
[2]ICT Convergence Research Division, Digital Healthcare Research Center, Gumi Electronics and Information
Technology Research Institute (GERI), Gumi 39253, South Korea
[3]Department of Biomedical Engineering, Ulsan National Institute of Science and Technology (UNIST), Ulsan 44919, South Korea
[4]Institute of Biomedical Engineering Research, Kyungpook National University, Daegu 41944, South Korea
[5]Department of Biomedical Engineering, College of Engineering, Kyungil University, Gyeongsan 38428, South Korea
[6]Center for Scientific Instrumentation, Korea Basic Science Institute, Daejeon 34133, South Korea
[7]Department of Nuclear Energy Convergence, Kyungil University, Gyeongsan 38428, South Korea
[8]Department of Autonomous Robot Engineering, College of Smart Engineering, Kyungil University, Gyeongsan 38428, South Korea

Corresponding author: Mansik Jeon (msjeon@knu.ac.kr)

ABSTRACT Large-scale product inspection is an important aspect in thin film industry to identify defects with a high precision. Although vision line scan camera (VLSC)-based inspection has been frequently implemented, it is limited to surface inspections. Therefore, to overcome the conventional drawbacks, there is a need to extend inspection capabilities to internal structures. Considering that VLSC systems have access to rich information, such as color and texture, high-resolution real-time multimodal optical synchronization between VLSC and dual spectral domain optical coherence tomography (SD-OCT) systems was developed with a laboratory customized in-built automated defect-tracking algorithm for optical thin films (OTFs). Distinguishable differences in the color and texture of the bezel area were precisely determined by the VLSC. Detailed OCT assessments were conducted to verify the detection of previously unobtainable border regions and micrometer-range sub-surface defects. To enhance the accuracy of the method, VLSC images were aided for the precise surface defect identification using OCT and the image acquisition, signal processing, image analysis, and classification of both techniques were simultaneously processed in real-time for industrial applicability. The results demonstrate that the proposed method is capable of detecting and enumerating total number of defects in OTF samples with exceptional resolution and in a cost-effective manner facilitating wide area inspection for OTF samples.

INDEX TERMS Automatic optical inspection, machine vision, optical coherence tomography, optical films, parallel processing.

I. INTRODUCTION

Hyper-resolution and hyper-scale technologies are being researched actively, and manufacturing success, which is directly related to the profit, is being methodically managed for mass production [1], [2]. To attain maximum manufacturing success in competitive markets, manufacturers make large-scale investments in production facilities and explore new real-time technologies for the pre-inspection of final products for possible defects. Optical thin films (OTFs), touch-screen panels (TSPs), and liquid crystal displays (LCDs) have attracted attention in the smart-display-device manufacturing industry. The large-scale rapid production of these products has led to an increase in the fault occurrence rate in the final products, which can cause huge financial losses [3], [4]. In particularly, in the smartphone industry,

several lamination processes involving thin multiple layers (ranging in thickness from a few nanometers to a few tens of micrometers) are employed to produce the final product. Although the manufactured product is compact, its inspection is important for preventing products with a drastically degraded quality, which can result from defective raw materials and manufacturing errors, from reaching the market.

With the development of photo-electronics giant strides have been made in the development of charge-coupled device/complementary-metal-oxide-semiconductor-based machine vision inspection technology. Although vision inspection is limited to the assessment of the surface of a product and the results are subjective, it has become increasingly important for multidimensional analysis, online inspection, and component quality control, such as three dimensional (3D) contouring and gauging [5]–[8]. It can be useful for identifying air bubbles, dark/bright spots, defective lines, black matrix defects, and scratches on the product surface. Apart from machine vision inspection techniques, there has been considerable research on X-ray, photoluminescence, scanning electron microscope, transmission electron microscope, and electroluminescence imaging techniques. Owing to the difficulty in identifying micrometer-range sub-surface defects and the limited image resolution, most of these techniques can be used only for detecting topographical defects [9], [10]. Therefore, costly techniques, such as scanning electron microscopy and transmission electron microscopy, involving destructive sample sectioning have been employed to achieve the desirable visualization [11]–[13].

Since non-invasive techniques can overcome the drawbacks of existing inspection techniques, they have attracted significant attention in recent years. Optical coherence tomography (OCT) is a non-invasive medical imaging modality that provides cross-sectional real-time information with exceptional resolution, and it is a best-fit candidate for achieving reliable and accurate product inspection [14]–[16]. Although OCT has been majorly used in medical applications, owing to its high-resolution and non-destructive imaging capability, it has also been used in diverse industrial applications [17]–[19]. The use of OCT-based quantitative assessment for 3D defect inspection of TSPs has been demonstrated [20], [21]. Moreover, numerous studies have employed OCT for inspecting solar cells, glass defects, and in paper manufacturing [17], [22], [23]. The results of its application have sufficiently confirmed OCT as a promising industrial inspection technique that can accurately localize and characterize various defects on both surface and sub-surface of a product sample with ultrahigh resolution, which is considerably higher than the resolution of other existing non-destructive cross-sectional inspection techniques. Since a red-green-blue vision line scan camera (RGB-VLSC) can be used for the rapid identification of external bubbles, dark/bright spots, defective lines, black matrix defects, and sub-surface scratches, integrating RGB

vision inspection with gray-scale OCT can provide an effective solution for increasing the speed as well as precision of product inspection. OCT has been employed in various multimodal applications for medical diagnosis [24]. Nevertheless, OCT-based multimodal imaging techniques have not been experimentally tested or studied in detail for industrial applications.

In this study, a multiprocessor based VLSC system was synchronized and integrated with OCT to realize a multimodal imaging inspection system with parallel architecture for inspecting OTF samples for defects. A thorough inspection was simulated by acquiring external surface images, cross-sections, 3D renders, and *en face* visualizations simultaneously in real-time in order to fully exploit the potential of the developed VLSC–Dual-OCT system and to identify the defect locations. The OCT field of view was increased using dual OCT inspection arms, and data processing was performed using a graphics processing unit (GPU) for synchronizing the VLSC and OCT and increasing the data processing speed. Here, the primary conceptual breakthrough is the mutual compensation of over kill inspection drawback of vision system and time consuming wide-area inspection OCT by systematic synchronization of two imaging techniques (VLSC-Dual-OCT). The secondary insight is the VLSC-assisted OCT inspection procedure based on image and signal processing methods, where the VLSC detects external defects and provides information on defect localization and potential defect locations for OCT. Since vision inspection operates with a high-speed and OCT can distinguish actual defects from apparent defects on both surface and sub-surface with an exceptional resolution, the main drawbacks of both systems, such as over kill operation and challenging wide are scanning was compensated in an equal manner. Since the color-coated bezel area of an OTF sample hampers broadband light transmission, the VLSC can be useful for the inspection of OTF samples. The performance of the integrated system was validated using a customized OTF sample with structures based on light-scattering parameters, geometrical shapes, dimensional parameters, and refractive index of a real sample. An automated defect detection algorithm was part of our inspection scheme for enumerating and demarcating the magnitudes and locations of defects rigorously; the scheme facilitates immediate real-time verification of whether a product is defective.

II. MATERIALS AND METHODS
A. CONFIGURATION OF VLSC-DUAL-OCT SYSTEM
Fig. 1 shows a schematic of the developed VLSC-Dual-OCT multimodal system, emphasizing the parallel architecture consisting of the VLSC system synchronized with the dual SD-OCT inspection arms. In the multimodal imaging system, the VLSC with RGB channels was an optical line scan camera (P4-CC-04K07T, 70 kHz, Teledyne DALSA, Canada) with an acquisition rate of 70 kHz. The acquired image data were acquired using a frame grabber (Solios eV-CL, Matrox, Dorval, Canada) and stored in a computer [25]. The frame
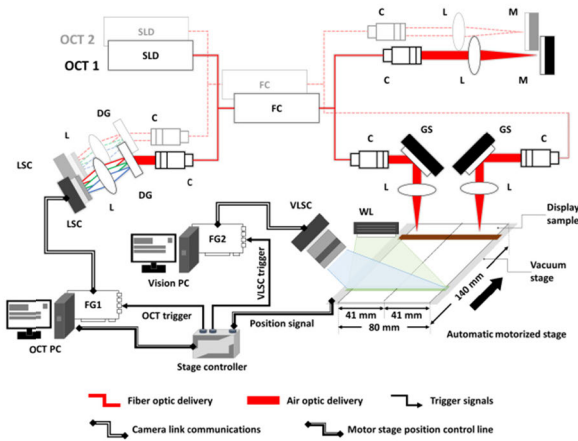
FIGURE 1. Configuration and operation procedure of the VLSC-Dual-OCT system. The expanded forms of the abbreviations are as follows: C: collimator, DG: diffraction grating, FC: fiber coupler, FG1 and FG2: frame grabber, GS: galvanometer scanner, L: lens, LSC: line scan camera, M: mirror, SLD: superluminescent diode, VLSC: vision line scan camera, and WL: white light.

grabbers of both VLSC and dual SD-OCT engines were connected to the translation stage controller (TS-P, Yamaha, Japan) to simply synchronize the initial trigger signals of the VLSC, OCT system, and translation stage. The illumination for the VLSC was provided by a serially installed special lighting device that radiated intense white light. The white light illumination (Fiber Optic Light Lines, Envision, South Korea) of the systems was customized according to the illumination requirements, with a field of view of 80 mm and a focal length of 50 mm. In order to receive information and images regarding defects from VLSC and to synchronize them with OCT assessments, the data stored in both VLSC computer and OCT computer were shared in real time via an online router (ipTIME H6005-IGMP, EFM Networks, South Korea). In the OCT configuration, dual superluminescent diodes (EXS210068-01, Exalos AG Ltd., Schlieren, Switzerland) with a wavelength centered at 840 nm and with a 55 nm bandwidth were used in both SD-OCT engines. The axial and lateral resolutions of both OCT engines were 7 and 20 μm, respectively. As shown in Fig. 1, the display sample was scanned parallel using the dual SD-OCT inspection arms to acquire a total scanning range of 80 mm from both inspection arms, with a 2 mm overlapping distance. The detailed information of the optical configuration can be found elsewhere [21]. To obtain 3D volume renders, the sample was moved perpendicularly to the 2D scanning directions using motorized translation stages (MF7, Yamaha, Japan) to obtain volume renders. The total area of a single 3D scan was 80 mm × 140 mm.

B. PARALLEL INSPECTION SOFTWARE ARCHITECTURE OF VLSC-DUAL-OCT

Fig. 2 depicts a descriptive operational flow chart, including data acquisition, image processing, signal processing, and defect tracking, of the developed VLSC system. The operational software of the VLSC-based inspection method
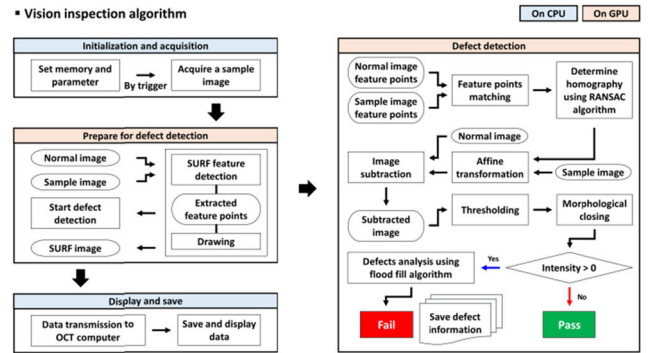
FIGURE 2. Flow chart representation of the software architecture of the VLSC inspection system for tracking defects.

was built on Microsoft Foundation Class by using Open Computer Vision on Visual Studio 2013. Two-dimensional (2D) surface images were acquired consecutively by using the VLSC, and they consisted of 8000 lines. Image processing and signal processing were performed using the Compute Unified Device Architecture (CUDA) cores of the GPU [26], [27]. As the first step of the inspection procedure, a defectless normal OTF sample was examined as a reference to verify the light-scattering parameters, geometrical shapes, and dimensional parameters of a normal sample. Thus, a sample verified as normal (by the manufacturer) was inspected using the VLSC. Vision-inspection-based feature extraction of the normal sample was performed using the speeded up robust features (SURF) algorithm, which was performed according to a method reported in [28]. Once feature extraction was accomplished, the obtained feature information of the bezel regions was stored in the system for reference. Next, a similar inspection was performed for the customized OTF sample (defective OTF sample). After the feature extraction of the objective sample, feature locations were matched between the normal and the customized samples to generate a homography (H) and to align the images of the samples in an overlapping manner. The homography was generated using the random sample consensus (RANSAC) algorithm [29]. Once the images were aligned, the intensities of the two customized sample image was subtracted from the normal OTF reference image and noise signals were removed to obtain the accurate intensity values, which corresponded to defect regions. Here, the morphological closing operator was used to erase unwanted or noise regions included in the selected regions, since they could adversely affect the inspection result [30], [31]. In the closing operator step, two operators—erosion and dilation—were used. As the initial procedure, dilation was first performed on the image and it was followed by erosion. It is operated or applied by multiplying each value of the structuring element with the pixel of the input image. The utilized shape for the structuring element was an ellipse (5 pixel × 5 pixel), and the number of iterations of Erode and Dilate was 3. The flood fill algorithm mentioned in the flow chart examines the dimensions of the leftmost, rightmost, top, and bottom four pixels of the detected defect regions to classify the defects.

For the accurate estimation of the defect locations on the OTF sample, a segmentation algorithm was developed to distinguish different interfaces of the OTF surface in the images acquired through the VLSC. As illustrated in Figure 2, CPP was used to cooperate CPU with GPU and to acquire image data, since the entire hardware architecture is operated using C++ language. This enables the role distribution between CPU and GPU as CUDA programming enables signal processing in complex image processing algorithms. One of the main advantages of CUDA is the compatibility with C language. Thus, functions of C language, which are compatible with C++ and CUDA codes were linked to communicate efficiently. Moreover, data can be copied simply through CUDA Memory of CUDA Runtime API to transfer data between main memory and GPU memory. As a result of C language compatibility of API of Frame grabber, the acquired data is stored in main memory through DMA (direct memory access) or the frame grabber memory is transferred from buffer to main memory. Since it is difficult to save data from GPU to HDD or SDD, the data acquisition part of camera and acquired data were presented in CPU, while the GPU signals were processed through the algorithm to balance the load between CPU and GPU. To divide the parallel tasks within GPU, a single CUDA thread was used to process a single pixel, while 256 threads per block were used. The number of blocks for a grid was depended on the image dimensions, and a single grid was utilized. In CUDA Programming, parallel operation is automatically performed using threads per block dimensions and image dimensions. Data between CPU and GPU is transmitted in two ways. Memory Host (Main memory) to Device (GPU memory) and Memory Device to Host. The final defect inspection result is displayed on the screen and the sample classification (upon defective or non-defective) is performed using robots in the production line.

Fig. 3 depicts a graphical representation of the data processing flow diagram of the developed segmentation algorithm. Data processing was initiated by uploading the normal OTF reference image and the VLSC image of the sample as inputs to the algorithm. The regions with the letters of the bezel area were used as the regions of interest for feature detection. Once feature detection was completed, well-matched feature points were connected for performing a precise comparison. The homography (H) obtained using the RANSAC algorithm, is followed by an affine transformation of the customized sample image. The intensity of the transformed image was subtracted from that of the normal OTF reference image to obtain the intensity difference between the two images. The intensity difference indicated the defect locations, where the upper image illustrated after image difference in the algorithm was acquired prior to image alignment and below image was acquired after the reference and sample images were accurately aligned intensities were subtracted.

The operational flow chart of SD-OCT is shown in Fig. 4. Windows Presentation Foundation, Visual Studio 2012, and
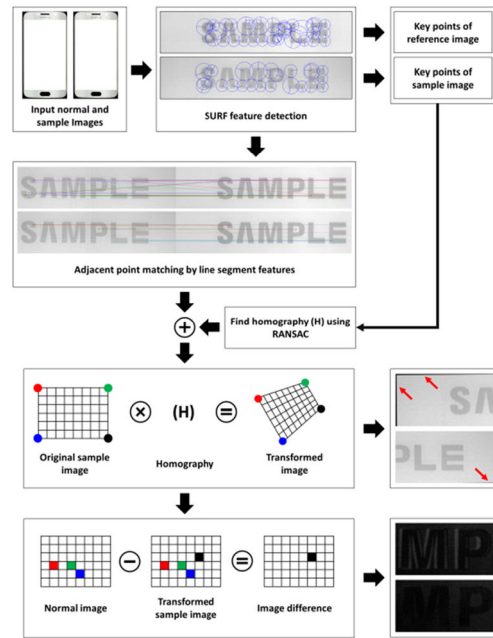

FIGURE 3. Graphical representation of the segmentation algorithm and defect identification.
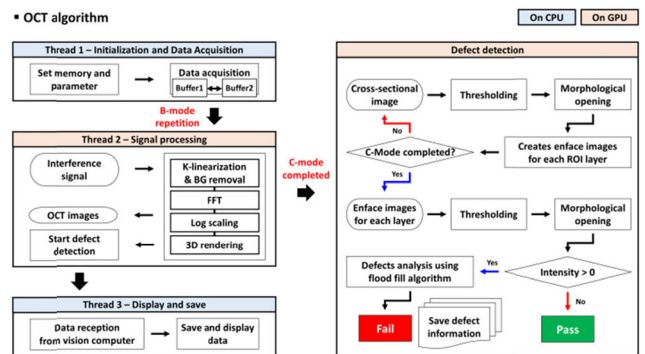

FIGURE 4. Flow chart representation of the parallel inspection software architecture of the SD-OCT system for detecting defects.

CUDA 6.5 were used to build the operational software. As shown in the figure, three threads were used for data acquisition, signal processing, and 2D and 3D image storage. The data acquisition thread first stored incoming 2D raw signals in the first buffer allocated in the host memory and then called the signal processing thread. Thereafter, the self-iterated acquisition thread continually transferred the incoming signals into the second buffer without any temporal delay between successive acquisition events. The signal processing thread extracted the frame data stored in the buffers of the host memory. Wavenumber (k)-domain linearization was achieved by performing full-range k-domain linearization, and this was followed by background removal, fast Fourier transform (FFT), log scaling, and 3D rendering. The reconstructed images were transferred to the host memory for being displayed. The frame rate of the SD-OCT system was increased by employing this rapid image processing procedure. For the detection of defects with the SD-OCT system, individual pixel-intensity-dependent thresholding was

performed to exclude the speckle noise of 2D-OCT images and to mosaic adjacent OCT image pixels. Adjacent OCT pixels were mosaicked using a morphological opening operator. The adjacent regions of the sample were imaged using OCT and the acquired images were optically aligned, merged using mosaicking technique, and loaded into a single memory. The dimension of one of the mosaicked block was 4000 pixels of width and 8000 pixels of height. Once the aforementioned thresholding and mosaicking were completed, 3D renders of the region of interest were employed to generate depth-dependent *en face* visualizations, and this was followed by thresholding by using a procedure similar to that used for the aforementioned thresholding. Once the thresholding of both 2D-OCT and OCT-*en face* images was completed, the remaining intensity signals of images demarcated the defect regions. The adjacent pixel information corresponding to the remaining intensity signals was precisely predetermined to distinguish the defects with the flood fill algorithm [32]. For the approximation of defect dimensions, either sides, the topmost region, the deepest region of the acquired cross-sections as well as *en face* visualizations were examined. In Figure 4, the parallel inspection software interface consists of three CPU threads, where thread 1; data acquisition thread, thread 2; commands GPU for image processing, thread 3; image construction and saving the image. CUDA threads will be allocated for GPU upon the image dimensions. Whenever, a single A-line is acquired, signal processing is performed in GPU. However, the efficiency of the process is degraded due to the large time consumption for data sharing between CPU and GPU. Since the signal processing of a complete C-mode image consumes more time and further degrades the efficacy, each B-mode signal has to be processed at each attempt of acquisition. Therefore, GPU was involved to avoid the data overflows between CPU threads and to process signals of 3D voxels directly.

C. DESCRIPTION OF THE VLSC-DUAL-OCT SYSTEM'S USER INTERFACE

Fig. 5 depicts the user interface of the developed VLSC-Dual-OCT imaging inspection system. Fig. 5(a) shows the OCT-*en face* visualization of the inspected sample. The red color rectangular boxes indicate defect candidates in the view area, and the white color rectangular box indicates the current inspection region. Figs. 5(b) and 5(c) show real-time cross-sectional and volumetric visualizations correspond to the region in the white color rectangular box region indicated in Fig. 5(a).

The results acquired by using the VLSC can be examined for surface defects in the vision inspection view. Fig. 5(e) shows the final OCT-VISION hybrid image with the defect regions that have been confirmed on the basis of the VLSC-Dual-OCT defect threshold parameters. In the process of thresholding, technical options, such as "binarization", "zeroing", and "inverting" were utilized. The acquired images were binarized and a predetermined threshold value was determined for the classification of defective regions.
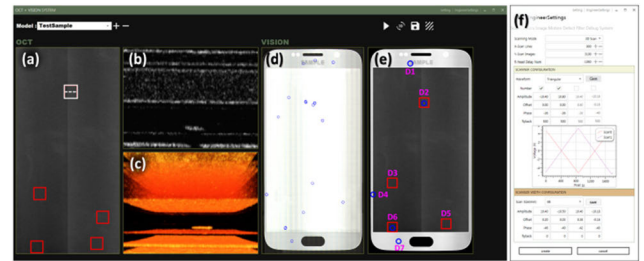
FIGURE 5. User interface of the VLSC-Dual-OCT system: (a) OCT *en face* view, (b) OCT cross-sectional view, (c) OCT 3D volumetric view, (d) vision inspection view, (e) OCT-VISION hybrid detection view, and (f) the OCT acquisition parameter settings panel.
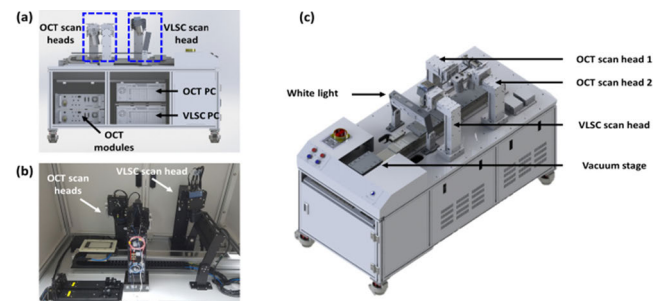

FIGURE 6. Pictorial overview of the developed VLSC-Dual-OCT system.

The regions, which were less than the predetermined threshold value were zeroed and the values beyond the predetermined threshold were inverted to 255. These predetermined threshold parameters of the defects were substantiated from LCD defect inspecting specifications reported in previous studies [19], [33], [34]. The operational parameters of the system are presented in Fig. 5(f), and they include the visual image size and scanning range of the sample. A pictorial overview of the final measurement setup and the systematic configuration for industrial application is shown in Fig. 6.

D. FABRICATION OF OTF SAMPLES WITH DELIBERATELY INTRODUCED DEFECTS

For the initial assessment and for the evaluation of the real-time inspection capability of the developed system, an OTF sample with embedded defects was fabricated. Fig. 7(a) depicts the structure of the OTF sample and provides the thickness of each layer and the vacuum gaps between the layers. The total thickness of the OTF was measured to be 700 μm, and the OTF consisted of a protective film (100 μm), a transparent film (250 μm), a deco film (150 μm), and a base film (100 μm). The thickness information of the vacuum gap between each aforementioned layer is indicated on Figure 7 (A). During the fabrication, defects were deliberately introduced by applying mechanical stress, using defective raw materials [35] in the protective film, bezel area, and view area. Fig. 7(b) shows a top view of the fabricated OTF. The dimensions of the OTF were measured to be 140 mm × 70 mm. Fig. 7(c) shows microscope images of the aforementioned defect locations, obtained with a Dino-Lite digital microscope (model no. AM4515ZT4, Taipei, Taiwan).
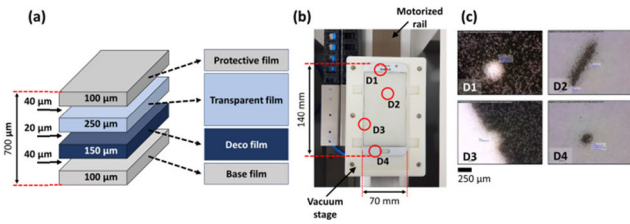
FIGURE 7. Graphical representation of the OTF customized fabricated sample, in which multiple defect regions were deliberately generated. (a) The classification and thickness information of the layers for the fabricated sample, (b) a top view of the OTF sample with defects (which are indicated by the labels D1–D4, and (c) microscope images of the defects shown in (b).
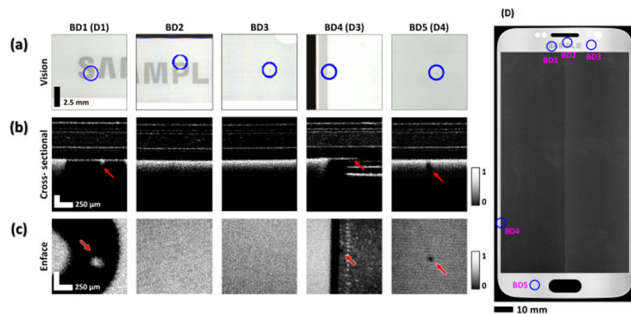
FIGURE 8. Acquired VLSC-Dual-OCT visualizations of the bezel area defect regions. Images in (a) are obtained using vision inspection system, (b) images are cross-sectional OCT images, (c) are *en face* OCT images obtained from the volumetric images, and (d) is the surface image of the sample obtained using vision camera. The labels BD1 –BD5 represent the five bezel area defects.

III. RESULTS

The developed VLSC-Dual-OCT multimodal system was examined for its capability to identify the location and the total detected size of defects in the bezel area of the OTF sample. Figure 8 depicts the VLSC-Dual-OCT hybrid visualizations of the defect regions in the bezel area. The bezel area was fabricated as an opaque colored region with printed letters. The results obtained through the VLSC were sufficient for identifying multiple millimeter-sized discoloration and barely apparent anomalies at the center and edges of the printed letters on bezel area. These anomalies reflected topographical defects, and the VLSC results shown in Fig. 8(a) localized these defects. Although the inspected sample material had a highly scattering nature, *en face* images from 2D and 3D-OCT volume scans of similar defect regions were acquired in a parallel manner by employing a synchronized signal provided by the VLSC, and its corresponding OCT cross-section and *en face* images are shown in Figs. 8(b) and 8(c). Fig. 8(d) presents a VLSC hybrid dual SD-OCT image showing the defect locations identified using the dual method. The identified defects are labeled as BD1–BD5 (bezel area defects 1–5) on the hybrid image. The obtained 2D-OCT and *en face* OCT results revealed anomalies in the structure formation in the sublayers with exceptional resolution. Thus, the proposed system can potentially help avoid the use of destructive techniques. Moreover, the graphical user interface of the system displays the word "Defective" sign in real-time when the acquired intensity and feature
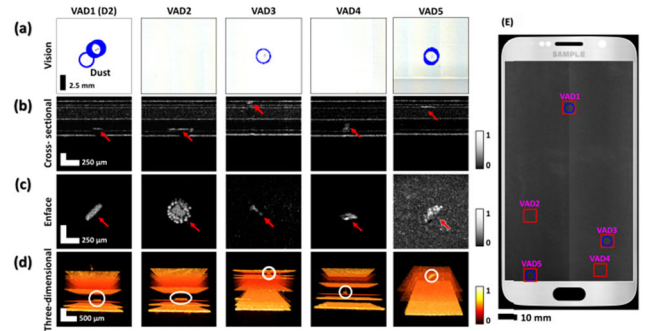
FIGURE 9. The acquired VLSC-Dual-OCT visualizations of the defect regions in the secondary view area. Images in (a) are obtained using vision inspection system, (b) are cross-sectional OCT images, (c) are *en face* OCT images showing the defects marked in (b) with red arrows, and (d) are the respective 3D volumetric OCT images. (e) *en face* representation.

parameters of both VLSC and dual SD-OCT are beyond the predetermined defect threshold values; it displays the word "Normal" otherwise. The red arrows in 2D-OCT and *en face* OCT- images with red arrows indicate accurately identified defect locations; these locations were notified as "Defective" by the user interface according to the predefined threshold parameters. The blue circles indicate the defect locations detected by the VLSC. The abbreviation BD stands for bezel area defect.

Fig. 9 shows the dual SD-OCT hybrid VLSC results for the secondary view area examined for defects. Since the defects were formed at the sub-surface of the OTF sample, only topographical information about the defects was provided by the VLSC, as shown in the images in Fig. 9(a). Owing to the transparency of the sample material in the view area, the OCT laser beam could successfully penetrate the sample material with less back-reflection. Thus, the sub layers and defects of the OTF were clearly identified.

The cross-sections revealed that the defects were located in a depth range of 10 to 600 μm. The defects were seen to form at a depth of 20 to 30 μm and grow slightly in size. Figs. 9(c) and 9(d) display the depth-dependent *en face* images and 3D volume renders of the identified defects, and Fig. 9(e) presents the hybrid image constructed using the VLSC and dual SD-OCT images. The image shows defect locations identified through the dual method. The identified defects are labeled as VAD1–VAD5 (view area defects 1–5) on the hybrid image. The increased scattering apparent at the defect locations could be due to a higher or lower density of the material relative to the surrounding regions, inclusions, or a higher concentration of specific raw materials relative to the surrounding regions. The slightly noisy appearance of the scans resulted from high scattering from the sub-layers. VAD1–VAD5 denote the five defects in the view area. The red arrows on the 2D and *en face* OCT images indicate the defect locations. The blue circles in (a) and (e) the red squares in indicates the defect locations classified by the VLSC and dual SD-OCT, respectively.

To further confirm the defect detection capability of the developed multimodal inspection system, precise localization

TABLE 1. Quantitative information on the sub-surface/surface location, depth, width, and height of each bezel area defect.

| Defect type	DEFECT PARAMETERS		
	LAYER	WIDTH [μM]	HEIGHT [μM]
DB (D1)	Deco film	40	40
DB2	Protective film	-	-
DB3	Protective film	-	-
DB4 (D3)	Deco film	20	20
DB5 (D4)	Deco film	20	20

TABLE 2. Quantitative information on the sub-surface/surface location, depth, width, and height of each defect in the view area.

Defect type	DEFECT PARAMETERS			
	LAYER	DEPTH [μM]	WIDTH [μM]	HEIGHT [μM]
VAD1 (D2)	Base film	42	240	240
VAD2	Base film	42	320	320
VAD3	Protective film	56	200	160
VAD4	Base film	126	220	120
VAD5	Transparent film	14	220	240

and dimension assessment were performed for the demarcated bezel and view area defects in the fabricated customized OTF sample. Tables 1 and 2 provide quantitative information about the exact location of the defects, their depth, and the subsurface layer, apart from 2D parameters (the width and height) of the classified defects. The width and height of the identified defects specified in the tables confirm the existence of defects on the surface and subsurface, and the quantitative approximation sufficiently reveals the exceptional resolution and non-destructive inspection capability of the developed multimodal inspection system.

IV. DISCUSSION

The proposed high-resolution VLSC helped identify the defect locations on the sample surface precisely, while SD-OCT facilitated the assessment of the subsurface abnormalities corresponding to the surface defects along with the overall inspection of the sample. Owing to the use of the VLSC, the exact defect locations to be scanned were readily known. This potentially increased the speed of inspection, which involved repeated measurements at multiple defect locations in the bezel and view areas (shown in Figs. 8 and 9). Since two types of optical imaging techniques were employed in the developed multimodal imaging inspection system, discrete defect tracking algorithms were developed. In the algorithms, defect regions and impurities with dimensions that were equal to or greater than the dimensions of a predefined
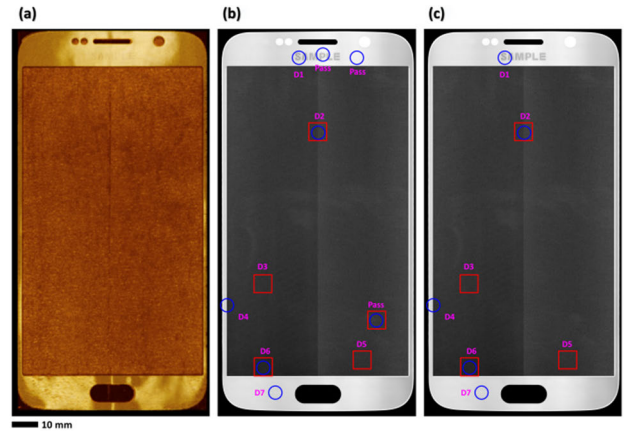
FIGURE 10. Acquired qualitative hybrid representation obtained by superimposing the OCT *en face* image on top of the VLSC visualization. (a) Is the 3D volumetric OCT images obtained from both sample arms, (b) is the surface view of the inspected sample obtained using vision camera, and (c) is the hybrid image obtained by superimposing the *en face* image extracted from the volumetric OCT image on top of surface image obtained using vision camera. The representation was used for the final classification of the verified defect locations.

defect threshold range were identified as defects, and foreign substances or structural abnormalities that could not be detected accurately underwent a re-inspection process for achieving clarity. For the evaluation of the reliability of the developed system and for the demonstration of its demarcation accuracy, the fabricated customized OTF samples with defects were examined several times. The obtained result is presented in Fig. 10 as a hybrid representation. Fig. 10(a) shows the rendered *en face* OCT image visualization and Fig. 10(b) depicts the OCT *en face* image superimposed on top of the VLSC visualization. The defect regions indicated by the VLSC (shown by the blue circles) and those detected by OCT (shown by red squares) correspond to both predefined "Normal" and "Defective" threshold parameter levels. Figure 10(c) shows the final classified qualitative hybrid representation, which provides precise confirmation of the defect locations according to predefined threshold parameters. The hybrid visualization reveals that defects that did not exceed the dimensions of the defect threshold parameters were excluded from the verified hybrid result. Thus, owing to the high sensitivity and high capability of the developed automated software-based intensity detection method, the defects were distinguished clearly in the verification performed using hybrid results of the VLSC and dual SD-OCT (shown in Figs. 8 and 9).

According to the best of our knowledge, real-time hybrid inspection attempts of both surface and sub-surface of OTFs using vision inspection integrated dual-OCT have been scarce. Therefore, one of the primary goals of this study was to confirm the feasibility of the developed optical inspection method for real-time defect localization and quantification of OTFs. Although related assessments were not descriptively studied, vision inspection based quantifications of previously reported defect inspection studies were well considered for baseline comparisons [36], [37]. In previous

studies [21], [35], [38]–[41], non-destructive identification of industrial materials has been achieved for diverse industrial materials. However, to date, a VLSC-synchronized with dual SD-OCT multimodal image inspection system for examining OTF sample defects in real time has not been studied in detail. Although numerous non-destructive techniques have been developed for similar tasks, the VLSC-Dual-OCT system presented here has considerable advantages over conventional methods. The main contribution of this study is the integration of two imaging techniques and the corresponding dual defect tracking algorithms for the effective inspection of the entire surface and sub-surface of OTF samples. And the obtained inspection results using laboratory customized OTF with sub-surface defects confirmed the feasibility of the developed defect inspection methodology for industrial applications convincing the technical rationale. The proposed integrated system is ideal for use in the mobile phone and LCD industries for pre-inspection of final products to identify possible defects. Although the developed multimodal system is bulky, it can help avoid subjective human errors, reduce inspection costs, and enhance product quality. Moreover, the conceptual innovation of the developed vision-synchronized dual-OCT inspection method is the equal compensation of the over kill inspection drawback of vision system and time consuming wide-area inspection OCT. Although vision inspection modality operates in a moderately high-speed, distinguishing of actual defects and apparently defects (fault defects) is a challenging task, which eventually leads to over kill inspection producing inaccurate error results. Moreover in the current demonstration, the minimum size of defects was determined as 100 μm with a standard refractive index. However to obtain results with a high precision and identify defects in each subsurface layer, the refractive index of each subsurface layer has to be considered. The mismatch of these refractive indexes can lead to scattering effects, which can mislead the dimensions of the defective regions that has to be further enhanced. Since OCT is potentially capable of distinguishing actual defects and apparent defects on both surface and sub-surface with an exceptional resolution, the results obtained through over kill inspection of vision system were directly undergone on cross-sectional and volumetric inspection to classify the actual defects from apparent defects. Hence as a result of this hybrid inspection protocol (vision-dual OCT inspection), considerable actual defective regions were well-confirmed with a high precision compared to sole operation of vision system, while overcoming the inspection speed limitation of a wide area using OCT system.

V. CONCLUSION

A high-resolution real-time VLSC-Dual-OCT multimodal imaging inspection system employing defect tracking algorithms was developed to distinguish complex surface as well as sub-surface defects from simplex defects. The advantage of the developed segmentation algorithm is that it can identify complex differences on the basis of intensity differences.

The algorithm precisely analyzed theoretically and through quantitative measurement. Laboratory customized defective OTF sample was used to verify the system performance. The qualitative and quantitative results precisely revealed and demarcated defect locations in both bezel and view areas of the OTF sample. Owing to its non-destructive nature and the use of multiple inspection parameters with high image resolution, the developed inspection system is expected to stand out when considered along with various conventional industrial inspection techniques. The acquired 2D volume visualizations and quantifications confirmed the desired results by compensating the ultimate limits of the existing techniques. It is expected that with its exceptional resolution and sensitivity, the developed VLSC-Dual-OCT technique will mature as an inspection technique and eventually be refined, evolving into an important high-performance inspection tool for the investigation of various types of defects in the LCD and mobile phone industries.

REFERENCES

[1] S.-H. Huang and Y.-C. Pan, "Automated visual inspection in the semiconductor industry: A survey," *Comput. Ind.*, vol. 66, pp. 1–10, Jan. 2015.

[2] A. Kumar, "Computer-vision-based fabric defect detection: A survey," *IEEE Trans. Ind. Electron.*, vol. 55, no. 1, pp. 348–363, Jan. 2008.

[3] X. Bi, C. Zhuang, and H. Ding, "A new mura defect inspection way for TFT-LCD using level set method," *IEEE Signal Process. Lett.*, vol. 16, no. 4, pp. 311–314, Apr. 2009.

[4] Y.-G. Cen, R.-Z. Zhao, L.-H. Cen, L.-H. Cui, Z.-J. Miao, and Z. Wei, "Defect inspection for TFT-LCD images based on the low-rank matrix reconstruction," *Neurocomputing*, vol. 149, pp. 1206–1215, Feb. 2015.

[5] J. Yang, X. Li, X. Xu, Y. Cao, Y. Zhang, L. Wang, and S. Jiang, "Development of an optical defect inspection algorithm based on an active contour model for large steel roller surfaces," *Appl. Opt.*, vol. 57, pp. 2490–2498, Apr. 2018.

[6] X. Feng, R. Su, T. Happonen, J. Liu, and R. Leach, "Fast and cost-effective in-process defect inspection for printed electronics based on coherent optical processing," *Opt. Express*, vol. 26, no. 11, pp. 13927–13937, 2018.

[7] R. Stojanovic, P. Mitropulos, C. Koulamas, Y. Karayiannis, S. Koubias, and G. Papadopoulos, "Real-time vision-based system for textile fabric inspection," *Real-Time Imag.*, vol. 7, no. 6, pp. 507–518, Dec. 2001.

[8] A. Baykut, A. Atalay, A. Erçil, and M. Güler, "Real-time defect inspection of textured surfaces," *Real-Time Imag.*, vol. 6, no. 1, pp. 17–27, Feb. 2000.

[9] R. Søndenå, Y. Hu, M. Juel, M. S. Wiig, and H. Angelskår, "Characterization of the OSF-band structure in n-type cz-Si using photoluminescence-imaging and visual inspection," *J. Cryst. Growth*, vol. 367, pp. 68–72, Mar. 2013.

[10] D.-M. Tsai, S.-C. Wu, and W.-Y. Chiu, "Defect detection in solar modules using ICA basis images," *IEEE Trans. Ind. Informat.*, vol. 9, no. 1, pp. 122–131, Feb. 2013.

[11] K. Tsujimoto, S. Tsuji, K. Kuroda, and H. Saka, "Transmission electron microscopy of thin-film transistors on glass substrates," *Thin Solid Films*, vol. 319, nos. 1–2, pp. 106–109, Apr. 1998.

[12] L. Meng, D. Nagalingam, C. S. Bhatia, A. G. Street, and J. C. H. Phang, "Distinguishing morphological and electrical defects in polycrystalline silicon solar cells using scanning electron acoustic microscopy and electron beam induced current," *Sol. Energy Mater. Sol. Cells*, vol. 95, no. 9, pp. 2632–2637, Sep. 2011.

[13] R. Nakagaki, T. Honda, and K. Nakamae, "Automatic recognition of defect areas on a semiconductor wafer using multiple scanning electron microscope images," *Meas. Sci. Technol.*, vol. 20, no. 7, Jul. 2009, Art. no. 075503.

[14] A. F. Fercher, "Optical coherence tomography," *J. Biomed. Opt.*, vol. 1, no. 2, pp. 157–173, Apr. 1996.

[15] A. G. Podoleanu, "Optical coherence tomography," *J. Microscopy*, vol. 247, no. 3, pp. 209–219, Sep. 2012.

[16] M. A. Choma, M. V. Sarunic, C. Yang, and J. A. Izatt, "Sensitivity advantage of swept source and Fourier domain optical coherence tomography," *Opt. Express*, vol. 11, no. 18, pp. 2183–2189, 2003.

[17] Z. Chen, Y. Shen, W. Bao, P. Li, X. Wang, and Z. Ding, "Identification of surface defects on glass by parallel spectral domain optical coherence tomography," *Opt. Express*, vol. 23, no. 18, pp. 23634–23646, 2015.

[18] M.-T. Tsai, F.-Y. Chang, Y.-J. Lee, J.-D. Lee, H.-C. Wang, and C.-K. Lee, "Defect detection and property evaluation of indium tin oxide conducting glass using optical coherence tomography," *Opt. Express*, vol. 19, no. 8, pp. 7559–7566, Apr. 2011.

[19] S.-H. Kim, J.-H. Kim, and S.-W. Kang, "Nondestructive defect inspection for LCDs using optical coherence tomography," *Displays*, vol. 32, no. 5, pp. 325–329, Dec. 2011.

[20] N. H. Cho, K. Park, J.-Y. Kim, Y. Jung, and J. Kim, "Quantitative assessment of touch-screen panel by nondestructive inspection with three-dimensional real-time display optical coherence tomography," *Opt. Lasers Eng.*, vol. 68, pp. 50–57, May 2015.

[21] M. Shirazi, K. Park, R. Wijesinghe, H. Jeong, S. Han, P. Kim, M. Jeon, and J. Kim, "Fast industrial inspection of optical thin film using optical coherence tomography," *Sensors*, vol. 16, no. 10, p. 1598, Sep. 2016.

[22] M.-T. Tsai, F.-Y. Chang, Y.-C. Yao, J. Mei, and Y.-J. Lee, "Optical inspection of solar cells using phase-sensitive optical coherence tomography," *Sol. Energy Mater. Sol. Cells*, vol. 136, pp. 193–199, May 2015.

[23] T. Prykäri, J. Czajkowski, E. Alarousu, and R. Myllylä, "Optical coherence tomography as an accurate inspection and quality evaluation technique in paper industry," *Opt. Rev.*, vol. 17, no. 3, pp. 218–222, May 2010.

[24] N. Vogler, A. Medyukhina, I. Latka, S. Kemper, M. Böhm, B. Dietzek, and J. Popp, "Towards multimodal nonlinear optical tomography–experimental methodology," *Laser Phys. Lett.*, vol. 8, p. 617, Jun. 2011.

[25] M. Nayyerloo, J. G. Chase, A. Millane, C. Muller, A. Malherbe, X.-Q. Chen, and G. A. MacRae, "Seismic structural displacement measurement using a line-scan camera: Camera-pattern calibration and experimental validation," *J. Civil Struct. Health Monitor.*, vol. 1, nos. 3–4, pp. 113–124, Dec. 2011.

[26] Z. Hocenski, T. Matic, and I. Vidovic, "Technology transfer of computer vision defect detection to ceramic tiles industry," in *Proc. Int. Conf. Smart Syst. Technol. (SST)*, Oct. 2016, pp. 301–305.

[27] M. Chang, B.-C. Chen, J. L. Gabayno, and M.-F. Chen, "Development of an optical inspection platform for surface defect detection in touch panel glass," *Int. J. Optomechatronics*, vol. 10, no. 2, pp. 63–72, Apr. 2016.

[28] N. K. Verma, A. Goyal, A. H. Vardhan, R. K. Sevakula, and A. Salour, "Object matching using speeded up robust features," in *Intelligent and Evolutionary Systems*. Cham, Switzerland: Springer, 2016, pp. 415–427.

[29] S. T. Teoh, M. Kitamura, Y. Nakayama, S. Putri, Y. Mukai, and E. Fukusaki, "Random sample consensus combined with partial least squares regression (RANSAC-PLS) for microbial metabolomics data mining and phenotype improvement," *J. Bioscience Bioeng.*, vol. 122, no. 2, pp. 168–175, Aug. 2016.

[30] M. Moraes, D. A. Cardenas, and S. Furuie, "Automatic lumen segmentation in IVOCT images using binary morphological reconstruction," *Biomed. Eng. OnLine*, vol. 12, no. 1, p. 78, 2013.

[31] T. M. Khan, M. Aurangzeb Khan, S. A. Malik, S. A. Khan, T. Bashir, and A. H. Dar, "Automatic localization of pupil using eccentricity and iris using gradient based method," *Opt. Lasers Eng.*, vol. 49, no. 2, pp. 177–187, Feb. 2011.

[32] J. Lee and H. Kang, "Flood fill mean shift: A robust segmentation algorithm," *Int. J. Control, Autom. Syst.*, vol. 8, no. 6, pp. 1313–1319, Dec. 2010.

[33] C. Jian, J. Gao, and Y. Ao, "Automatic surface defect detection for mobile phone screen glass based on machine vision," *Appl. Soft Comput.*, vol. 52, pp. 348–358, Mar. 2017.

[34] Z.-C. Yuan, Z.-T. Zhang, H. Su, L. Zhang, F. Shen, and F. Zhang, "Vision-based defect detection for mobile phone cover glass using deep neural networks," *Int. J. Precis. Eng. Manuf.*, vol. 19, no. 6, pp. 801–810, Jun. 2018.

[35] R. E. Wijesinghe, K. Park, Y. Jung, P. Kim, M. Jeon, and J. Kim, "Industrial resin inspection for display production using automated fluid-inspection based on multimodal optical detection techniques," *Opt. Lasers Eng.*, vol. 96, pp. 75–82, Sep. 2017.

[36] Y. Park and I. S. Kweon, "Ambiguous surface defect image classification of AMOLED displays in smartphones," *IEEE Trans. Ind. Informat.*, vol. 12, no. 2, pp. 597–607, Apr. 2016.

[37] K.-C. Chang Chien and H.-Y. Tu, "Complex defect inspection for transparent substrate by combining digital holography with machine learning," *J. Opt.*, vol. 21, no. 8, Aug. 2019, Art. no. 085701.

[38] M. F. Shirazi, R. E. Wijesinghe, N. K. Ravichandran, P. Kim, M. Jeon, and J. Kim, "Quality assessment of the optical thin films using line field spectral domain optical coherence tomography," *Opt. Lasers Eng.*, vol. 110, pp. 47–53, Nov. 2018.

[39] K. Kim, P. Kim, J. Lee, S. Kim, S. Park, S. H. Choi, J. Hwang, J. H. Lee, H. Lee, R. E. Wijesinghe, M. Jeon, and J. Kim, "Non-destructive identification of weld-boundary and porosity formation during laser transmission welding by using optical coherence tomography," *IEEE Access*, vol. 6, pp. 76768–76775, 2018.

[40] J. Lee, M. F. Shirazi, K. Park, M. Jeon, and J. Kim, "Defect inspection of actuator lenses using swept-source optical coherence tomography," *Opt. Rev.*, vol. 25, no. 3, pp. 403–409, Jun. 2018.

[41] M. Shirazi, M. Jeon, and J. Kim, "Structural analysis of polymer composites using spectral domain optical coherence tomography," *Sensors*, vol. 17, no. 5, p. 1155, May 2017.

DEOKMIN JEON received the B.E. degree in electronics engineering from Kyungil University, Gyeongsangbuk, South Korea, in 2014. He has been a Ph.D. Researcher with the Electronics Engineering Department, Kyungpook National University, Daegu, South Korea, since 2016. His research interests include development of novel biomedical and industrial imaging technique using advanced optical materials, including optical coherence tomography, vision inspection, photoacoustic imaging, and other optical applications.

UNSANG JUNG received the Ph.D. degree in electronics engineering from Kyungpook National University, Daegu, South Korea, in 2013. He was a Research Assistant Professor with the Department of Creative IT Engineering, Pohang University of Science and Technology (POSTECH), from 2014 to 2018. He was also a Principal Research Engineer with HPK Inc., in 2019. He is currently a Senior Researcher with the Gumi Electronics and Information Technology Research Institute (GERI). His research interests include development of optical imaging system techniques, including multiphoton microscopy, optical coherence tomography (OCT), camera vision imaging systems, application for medical and industrial fields, development of optical imaging systems, and signal processing algorithm for medical or industrial fields using imaging technology.

KIBEOM PARK received the Ph.D. degree from the Department of Electronics Engineering, Kyungpook National University, Daegu, South Korea, in 2018. He is also Researching and Developing of optical and biological system with the Institute of Biomedical Engineering, Ulsan National Institute of Science and Technology. His research interests include develop new optical technologies that address challenges in clinical medicine and basic biological research.

PILUN KIM received the Ph.D. degree from the Department of Medical and Biological Engineering, Kyungpook National University, in 2011. He is currently a Researching Visiting Professor with the Institute of Biomedical Engineering, Kyungpook National University. His research interests include translating new technologies from research field to application field, such as clinic and industrial and making its productization, biomedical device development, optical coherence tomography (OCT), and digital image processing.

SANGYEOB HAN is currently pursuing the Ph.D. degree with the School of Electronics Engineering, Kyungpook National University, Daegu, South Korea. His research interests include optical imaging techniques, photoacoustic microscopy, optical coherence tomography, and multiphoton microscopy.

HYOSANG JEONG received the M.S. degree in electronics engineering from Kyungil University, Daegu, South Korea. His research interests include optical imaging techniques, optical coherence tomography, optical Doppler tomography, general-purpose computing on graphics processing units, parallel algorithms, software architecture, and industrial applications.

RUCHIRE ERANGA WIJESINGHE received the B.Sc. and Ph.D. degrees in electronics engineering from Kyungpook National University, Daegu, South Korea, in 2012 and 2018, respectively. He is currently an Assistant Professor with the Department of Biomedical Engineering, Kyungil University. His research interests include development of high-resolution novel biological and biomedical imaging techniques, including optical coherence tomography and microscopy for clinical utility.

NARESH KUMAR RAVICHANDRAN received the B.E. degree in electronics and communication engineering from St. Peter's University, India, and the M.Sc. degree in electronics engineering from Kyungpook National University, Daegu, South Korea. He has been a Ph.D. Researcher with the Electronics Engineering Department, Kyungpook National University, since 2016. His research interests include developing and optimizing novel biological imaging techniques with possible applications in agronomical studies, entomological studies, industrial applications, and dental applications.

JAEYUL LEE is currently pursuing the Ph.D. degree with the School of Electronics Engineering, Kyungpook National University, Daegu, South Korea. His research interests include optical imaging techniques, photoacoustic microscopy, optical coherence tomography, handheld instruments for optimization of optical coherence tomography, and photoacoustic microscopy systems.

YOUNGMIN HAN received the B.E. degree in mechanical engineering from Tohoku University, Sendai, Japan, in 2012, and the M.Sc. degree in power engineering from the Technical University of Munich, Munich, Germany. His research interests include development of advanced materials, including tungsten metals and molten salts for nuclear fusion reactors using optical techniques and image processing.

MANSIK JEON (Member, IEEE) received the Ph.D. degree in electronics engineering from Kyungpook National University, Daegu, South Korea, in 2011. He is currently an Assistant Professor with the School of Electronics Engineering, Kyungpook National University. His research interests include development of nonionizing and noninvasive novel biomedical imaging techniques, including photoacoustic tomography, photoacoustic microscopy, optical coherence tomography, ultrasonic imaging, and handheld scanner and their clinical applications.

JEEHYUN KIM (Member, IEEE) received the Ph.D. degree in biomedical engineering from The University of Texas at Austin, USA, in 2004. He was a Postdoctoral Researcher with the Beckman Laser institute, University of California, Irvine. He is currently a Professor with Kyungpook National University, Daegu, South Korea. His research interests include biomedical imaging and sensing, neuroscience studies using multiphoton microscopy, photo-acoustic imaging, and other novel applications of sensors.

• • •